A predictive approach to simulating the forming of viscous textile composite sheet

Philip Harrison* — **Woong-Ryeol Yu**** — **Jinhuo Wang***** **Andrew C. Long***** — **Michael J. Clifford*****

** Department of Mechanical Engineering, James Watt Building (South), University of Glasgow, Glasgow G12 8QQ, U.K.*

philip.harrison@nottingham.ac.uk

*** School of Materials Science and Engineering, Seoul National University, Seoul, South Korea*

**** School of Mechanical, Materials and Manufacturing Engineering The University of Nottingham, University Park Nottingham NG7 2RD, U.K.*

ABSTRACT. *A commercial Finite Element (FE) code is used to simulate the forming of a thermoplastic viscous textile composite sheet. The main success of this work is in combining two distinct models. The first is a rate and temperature dependent unit cell energy model, designed to predict the shear force – shear angle – shear rate response of viscous textile composites. The second is a non-orthogonal rate-independent constitutive model that has been implemented previously in the code. Both models are reviewed briefly and the method of combining these models in the code is described. Preliminary results of Picture Frame test simulations together with complex forming simulations are presented and discussed.*

KEYWORDS: *forming, textile composites, rate-dependence.*

REEF – 14/2005. Composites forming simulation, pages 613 to 631

1. Introduction

Virtual technology is an important tool in improving efficiency in automated manufacturing processes. As such, deep drawing and press forming of viscous textile composites, including thermosetting prepregs and fabric reinforced thermoplastics, are prime candidates for virtual process development. Competition between composites and metals has created strong demand for such simulation technology in the composites industry, resulting in considerable research interest in the field. In the past, two main approaches have been followed in the forming simulation of textile composites, namely the development of algorithms based on pin-jointed net kinematics (Long, 1994; Robertson *et al*., 1981; Van West and Luby, 1997) which give a reasonable first order approximation to the forming behaviour of rate independent textile composites and the Finite Element (FE) method. The latter is potentially a more accurate method and can be used to simulate both rate independent (Boisse *et al*., 2001; Yu *et al*., 2002) and rate dependent or viscous behaviour (Hsiao and Kikuchi, 1999; Lamers *et al*., 2002a; 2002b; Picket *et al*., 1995). A difficulty in modelling viscous textile composites is often found to be in determining appropriate constitutive model material parameters. Hsiao and Kikuchi (1999) addressed this issue by using homogenisation methods enabling prediction of material rheology from parameters such as matrix viscosity and fibre volume fraction, though at the cost of computationally expensive numerical calculations. In this paper an alternative, economical method to predictive modelling of the forming behaviour of viscous textile composites is described and demonstrated.

A non-orthogonal constitutive model implemented previously in a commercial FE code, Abaqus Standard™ and Explicit™, (Yu *et al.,* 2002; 2003) is used to incorporate predictions from a constituent based unit cell energy model (Harrison *et al*., 2002; 2004a). As it stands this non-orthogonal model is rate-independent. However, by linking the shear parameters of the non-orthogonal model to predictions of the energy model, both rate and temperature effects can be included in the simulations. The main role of the energy model is to predict the shear force – shear angle – shear rate behaviour of viscous textile composites using material parameters supplied readily by material manufacturers, such as fibre volume fraction, weave architecture and matrix rheology. The motives for such constituent-based predictive modelling are two-fold. First, once the material behaviours of the constituent components are known then the rheology of any composite comprised of matrix and continuous inextensible fibres can be predicted, allowing the pre-manufacturing optimisation of a composite to suit a potential application. Second, characterising the rheological behaviour of, for example, a thermoplastic matrix polymer at different shear rates and temperatures is relatively easy using modern rheometers, compared with the equivalent but more difficult task of characterising the rheology of textile composites using picture frame and bias extension tests (Harrison *et al*., 2004b). Success in both these issues would lead to significant reductions in time and cost in the manufacturing process. The structure of this paper is as follows. The energy model is summarised followed by a brief description of the non-orthogonal model. Full descriptions of these models can be found elsewhere

(Harrison *et al*., 2002; 2004a, Yu *et al*., 2002; 2003). The method of incorporating predictions of the energy model in the non-orthogonal model is outlined. The general method is illustrated through discussion of implicit FE simulations of the Picture Frame test and explicit FE simulations of double-dome press forming operations.

2. Micro-mechanical model

During shear, it has been observed that the in-plane shear strain rate of tows is rarely as high as the overall in-plane shear rate across the composite sheet (Harrison *et al*., 2004a). This produces a discontinuous shear strain profile across the sheet with most of the shear strain concentrated in inter-tow regions. An example of such a non-linear shear profile is shown in Figure 1.

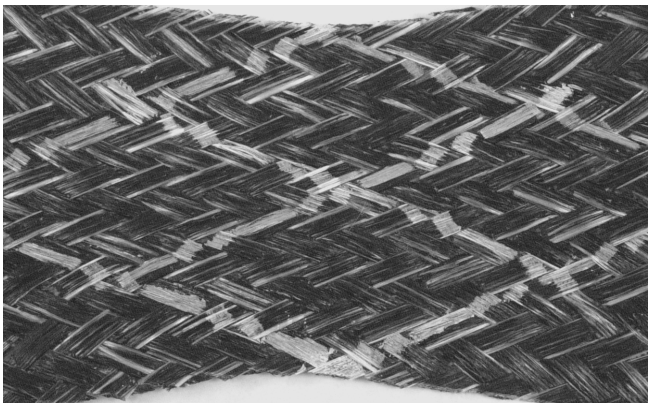

Figure 1. *Example of discontinuous shear strain profiles across a textile composite. The broken form of initially continuous lines drawn on the fabric before shear, serves to illustrate the strain profiles. 2 x 2 twill weave glass/polypropylene thermoplastic sheared in a bias extension test at 180^{o}C*

These observed kinematics (Harrison *et al*., 2002) have motivated the use of a novel two-phase material model structure to analyse the energy dissipation within the textile composite. For the purpose of the model, the textile is considered to consist of two distinct superposed layers, each consisting of parallel tows and inter-tow regions, see Figure 2. Each tow is modelled as a volume of uniaxial Ideal Fibre Reinforce Fluid (IFRF) whereas the inter-tow regions are filled with isotropic matrix fluid. The observed kinematics have important consequences for the deformation occurring during shear of textile composites, both within tow (fibre bundle) and inter-tow regions, and also between tow crossovers.

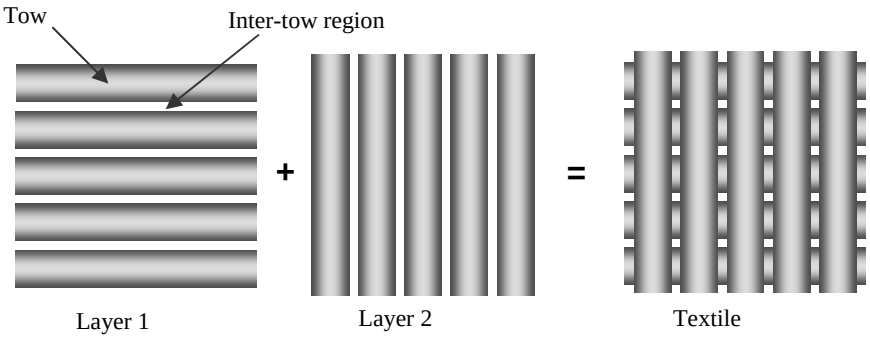

Figure 2. *Textile modelled as two superposed layers of uniaxial composite consisting of tow and inter-tow regions*

Considering, for example, the rate of deformation tensor, the discontinuous shear profile means that $2D_{ij}$ must be re-derived for both the tow and inter-tow regions. In order to do this it is necessary to define a set of coordinate systems, see Figure 3.

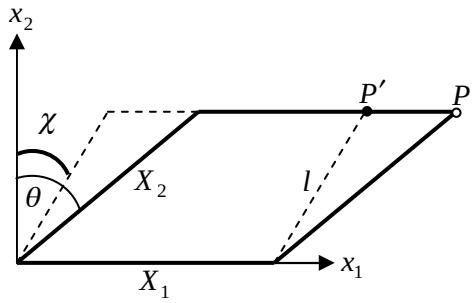

Figure 3. *Coordinate system.* θ *is the material shear angle,* χ *is the shear angle of this local region (indicated by dashed lines),* χ_t *when referring to the tow region or* χ_m *when referring to inter-tow region*

The first coordinate system, x_i, describes a fixed Cartesian system. A second material coordinate system, X_i, is considered attached to and to deform with each point, *P*, of a continuum in a hypothetical material undergoing homogeneous deformation. This is referred to here as the material coordinate system. Note that for the case of heterogeneous shear, particles of the localised continuum attached to the tows or inter-tow regions, referred to here by *P'*, are no longer stationary in the material coordinate system. Figure 3 shows the deformation imposed in the tow regions. In the case shown, χ corresponds to the tow shear angle, χ_t, where

$0 \le \chi_t \le \theta$ and where θ is the material shear angle. The derivation also applies to the inter-tow region, however, in that case, χ would correspond to the shear angle of the inter-tow region, χ_m. The fibre direction is considered parallel to the X_1 axis of the fixed frame. It can be shown that in this reference frame,

$$2D_{ij} = \begin{bmatrix} 0 & \left(\dot{\chi}\sec^2\chi - \dot{\theta}\tan\theta\tan\chi\right) & 0 \\ \left(\dot{\chi}\sec^2\chi - \dot{\theta}\tan\theta\tan\chi\right) & -2\dot{\theta}\tan\theta & 0 \\ 0 & 0 & 2\dot{\theta}\tan\theta \end{bmatrix} \quad [1]$$

where $\dot{\theta}$ is the relative angular velocity of the two reinforcement directions in the textile. From Equation [1] the simple shear rate of the tows or inter-tow regions, $\dot{\gamma}_t$ or $\dot{\gamma}_m$, is given as

$$\dot{\gamma} = \dot{\chi}\sec^2\chi - \dot{\theta}\tan\theta\tan\chi \quad [2]$$

where χ and $\dot{\chi}$ must be chosen accordingly to represent either the tow or inter-tow regions in order to calculate the shear rate, $\dot{\gamma}$, in the tow, $\dot{\gamma}_t$ or inter-tow, $\dot{\gamma}_m$, regions. From Equation [2] is can be shown that when $\dot{\chi} = \dot{\theta}$ at all times (the condition of homogeneous shear) then $\dot{\gamma} = \dot{\theta}$. Using tensor notation, the constitutive equation for a uniaxial IFRF (Rogers, 1989), is given by Equation [3]

$$\sigma_{ij} = -p\delta_{ij} + T_a a_i a_j + 2\eta_T D_{ij} + 2(\eta_L - \eta_T)(a_i a_k D_{kj} + a_j a_k D_{ki}) \quad [3]$$

where δ_{ij} denotes the unit tensor, a_i defines the direction of the fibre reinforcement, $-p\delta_{ij}$ and $T_a a_i a_j$ are reaction stresses due to the constraints of incompressibility and fibre inextensibility, η_T and η_L are the transverse and longitudinal viscosity parameters and *i*, *j* and *k* range from 1 to 3. Using micro-mechanical modelling principals (Christensen, 1993; Coffin, 1995) both η_T and η_L can be predicted from the matrix viscosity, η_m, and fibre volume fraction. The interaction between fibres and matrix occurs on a microscopic scale and is shown in the schematic of Figure 4. Here the transverse viscosity, η_T, results from individual fibres rolling past one another, while the longitudinal viscosity, η_L, results from the fibres sliding past one another along their length. Numerous ingenious experiments have been devised to measure these two viscosities (Martin *et al*., 1995; McGuiness *et al*., 1998; Shuler *et al*., 1996). It should be noted that, unlike the viscosity parameters appearing in uniaxial IFRF theory, viscosity parameters appearing in the constitutive equations of biaxial IFRF (McGuiness *et al*., 1997; Spencer, 2000) can

not each be identified with a particular well-defined deformation kinematic and so can not be related to micro-mechanical mechanisms. This precludes the possibility of developing constituent based models based on biaxial IFRF model theory.

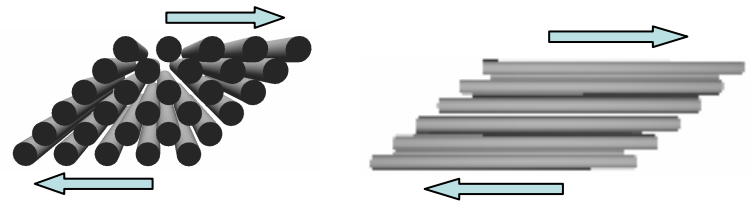

Figure 4. *(a) Shearing the composite across or transverse to the fibre direction gives a measure of the transverse viscosity and (b) shearing the composite parallel to the fibre direction gives a measure of the longitudinal viscosity*

Using Equation [1] and [3] together with the plane stress condition, it is possible to determine the rate of energy dissipation of the combined tow and inter-tow regions during shear using an expression for the stress power, dE/dt, of the deforming material (McGuiness *et al*., 1995),

$$\frac{dE}{dt} = W_o h\left(4\eta_T \dot{\theta}^2 \tan^2\theta + \eta_L \dot{\gamma}_t^2\right) + w_o hq\eta_m\left(4\dot{\theta}\tan^2\theta + \dot{\gamma}_m^2\right) \qquad [4]$$

where W_o and w_o are the initial widths of the tow and inter-tow regions, h is the thickness of the sheet, q is a factor related to the fabric architecture (*i.e*. the contact area between adjacent tows) and $\dot{\gamma}_t$ and $\dot{\gamma}_m$ are found using Equation [2]. However, while the analysis described above accounts for the energy dissipation within the tow and inter-tow regions, the heterogeneous strain profile also induces energy dissipation between the tow crossovers. The velocity field between crossovers is calculated by analysing the in-plane kinematics of tow deformation during shear (Harrison *et al*., 2002; 2004a). The resulting velocity field between crossovers is

$$\bar{v}_{rel} = \left\{\left(\dot{\gamma}_t - \dot{\theta}\right)(1-\sin\theta)Y\right\}\hat{\mathbf{i}} + \left\{\left(\dot{\theta} - \dot{\gamma}_t\right)(1-\sin\theta)X\right\}\hat{\mathbf{j}} \qquad [5]$$

where the unit vectors, $\hat{\mathbf{i}}$ and $\hat{\mathbf{j}}$ are orthogonal and coincide with the fibre reinforcement bisector directions and X and Y are the position coordinates in this reference frame. A polynomial function, Equation [6], can be fitted to the measured tow shear kinematics.

$$\chi_t = 1.72\times10^{-4}\theta^3 - 1.72\times10^{-2}\theta^2 + 0.7701\theta + 0.2311 \qquad [6]$$

The experimental measurements were made on a pre-consolidated 2 x 2 twill weave glass/polypropylene thermoplastic composite at various angular shear rates and using both Picture Frame and Bias Extension tests. By differentiating Equation [6] with respect to time and using Equation [2] it is possible to calculate the velocity field between the tow crossovers from Equation [5]. Future refinements of the model will allow prediction of the tow shear kinematics. Assuming that the thickness of the matrix film separating tows at the tow crossovers is the same as the distance separating individual fibres within the tows, the thickness of the matrix film can be estimated from the fibre volume fraction of the composite. Using the velocity field and matrix film thickness the shear strain rate in the matrix film can be estimated as a function of position. Finally, given the matrix viscosity, an estimate of the rate of energy dissipation can be determined due to shear between tow crossovers. By combining the energy contributions from both tow/inter-tow shear and crossover shear, the total rate of energy dissipation during shear of the textile composite can be estimated and from this the shear force can be determined. (Similar to equating the product of the axial force and the crosshead displacement rate of a Picture Frame test with the stress power of the test sample (McGuiness and O'Bradaigh, 1997)).

3. Non-orthogonal model

To model the stress and strain relationship dependent on the fibre directional properties, a non-orthogonal equation has been developed in an explicit mathematical form by using a homogenization method (Yu *et al.,* 2002). The resulting 2-D equation is based on a structural net concept (see Figure 5) and its derivation follows two distinct steps.

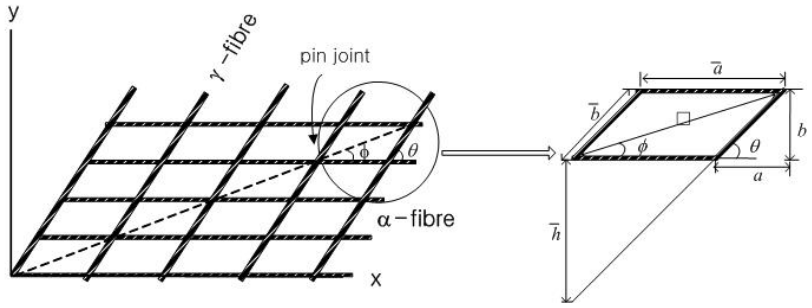

Figure 5. *A structural net (left) and unit cell (right) of fabric reinforcement*

Firstly, the contribution to total stress due to tensile strain in the non-orthogonal fibres is derived in a materially embedded orthogonal reference frame, with its *x*-axis co-linear with the fabric warp reinforcement direction (single dash system in Figure 6). The resulting tensile equation, Equation [7], relates incremental stress to

incremental strain in this reference system. In this first step of the derivation the warp and weft fibres are assumed to rotate freely at crossover contact points assuming no frictional resistance.

$$\begin{bmatrix} \Delta\sigma_{xx} \\ \Delta\sigma_{yy} \\ \Delta\sigma_{xy} \end{bmatrix} = \begin{bmatrix} \frac{\tilde{\tilde{E}}^{\alpha}}{bc} + \Gamma\left(\frac{a}{\bar{\bar{h}}}\right)\left(\frac{a^2}{c}\right) & \Gamma\left(\frac{a}{\bar{\bar{h}}}\right)\left(\frac{b^2}{c}\right) & \Gamma\left(\frac{a}{\bar{\bar{h}}}\right)\left(\frac{ab}{c}\right) \\ \Gamma\left(\frac{b}{\bar{a}}\right)\left(\frac{a^2}{c}\right) & \Gamma\left(\frac{b}{\bar{a}}\right)\left(\frac{b^2}{c}\right) & \Gamma\left(\frac{b}{\bar{a}}\right)\left(\frac{ab}{c}\right) \\ \Gamma\left(\frac{b}{\bar{\bar{h}}}\right)\left(\frac{a^2}{c}\right) & \Gamma\left(\frac{b}{\bar{\bar{h}}}\right)\left(\frac{b^2}{c}\right) & \Gamma\left(\frac{b}{\bar{\bar{h}}}\right)\left(\frac{ab}{c}\right) \end{bmatrix} \begin{bmatrix} \Delta\varepsilon_{xx} \\ \Delta\varepsilon_{yy} \\ 2\Delta\varepsilon_{xy} \end{bmatrix} \quad [7]$$

where $\Delta\sigma$ and $\Delta\varepsilon$ are the stress and strain increments, *a*, *b* and $\bar{\bar{h}}$ are related to the fabric geometry (see Figure 5), *c* is the sheet thickness and $\tilde{\tilde{E}}^{\alpha}$ and Γ are representative of the tensile stiffness of the warp and weft yarns (Yu *et al.*, 2002). In a second step, shear stress versus shear angle data is related to shear stiffness using a non-orthogonal analysis to find

$$\sigma_{12} = \frac{F_s}{lh}\left(\sqrt{g^{11}}\mathbf{g}_1 \otimes \mathbf{g}_2 + \sqrt{g^{22}}\mathbf{g}_2 \otimes \mathbf{g}_1\right) \quad [8]$$

where F_s is the shear force, $\hat{\mathbf{g}}_1$ and $\hat{\mathbf{g}}_2$ are unit covariant base vectors that convect with the warp and weft fibre directions (see Figures 6 and 7), *l* is the side length of the material and g^{ij} are components of the conjugate tensor.

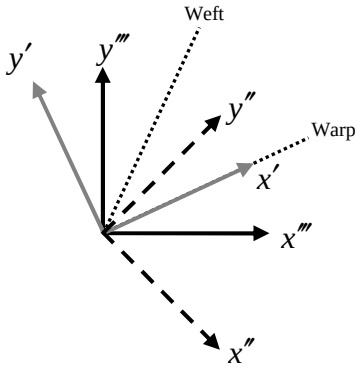

Figure 6. *Warp and weft fibre reinforcement directions plus three orthogonal reference frames used in analysis. Single dashed system has x-axis collinear with warp reinforcement direction (reference frame of Equation [7]). Double dashed system bisects the two fibre directions (reference frame of Equation [10]). Triple dashed system is material reference frame used in FE analysis (Equations [7] and [10] are transformed to this system before addition)*

The incremental stress due to shear is then calculated by linearising the stress equation, *i.e.*

$$\Delta\sigma_{ij} = \frac{d\sigma_{ij}}{d\theta}\Delta\theta \qquad [9]$$

where $d\sigma_{ij}/d\theta$ is the tangent stiffness matrix. Equation [9] is then transformed into the orthogonal fibre bisector frame (double dash system shown in Figure 6) and related to the fibre shear angle increment, $\Delta\theta$, as

$$\Delta\boldsymbol{\sigma} = \begin{bmatrix}\Delta\sigma_{xx}\\ \Delta\sigma_{yy}\\ \Delta\sigma_{xy}\end{bmatrix} = \begin{bmatrix}0 & 0 & 2G_1 g_1^1 g_2^1 + G_2\left(g_1^1 g_2^2 - g_1^2 g_2^1\right)\\ 0 & 0 & 2G_1 g_1^2 g_2^2 + G_2\left(g_1^1 g_2^2 - g_1^2 g_2^1\right)\\ 0 & 0 & G_1\left(g_1^1 g_2^2 + g_2^1 g_1^2\right)\end{bmatrix}\begin{bmatrix}0\\ 0\\ \Delta\theta\end{bmatrix} \qquad [10]$$

where G_1 and G_2 are model parameters that can be related explicitly to the shear force versus shear angle curve and g_1^1, g_1^2 are components of $\hat{\mathbf{g}}_1$ expressed in the orthogonal fibre bisector frame (double dashed system in Figure 6). Similarly, g_2^1, g_2^2 are components of $\hat{\mathbf{g}}_2$ (Yu *et al.*, 2003).

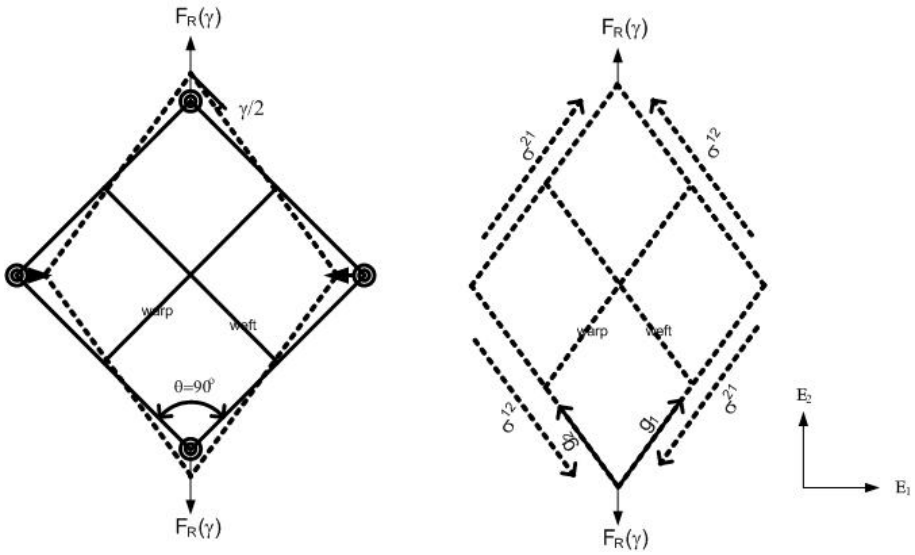

Figure 7. *Schematics of the picture-frame shear test (left) and contra-variant stress (σ^{12}, σ^{21}) components acting along normalized covariant based vectors ($\mathbf{g}_1, \mathbf{g}_2$). The unit vectors **E**$_1$ and **E**$_2$ are co-linear with the double-dashed system of Figure 6*

Equations [7] and [10] are both rotated into the materially embedded reference frame used by the FE code (triple dash system in Figure 6), *via* a user subroutine. The stress increments calculated by these rotated equations are then simply added together to find the final combined stress in this materially embedded reference system. An attractive feature of this non-orthogonal model is that, given the shear angle the two shear parameters G_1 and G_2 can be related analytically to the shear force versus shear angle response of textile composites through Equations [11] and [12].

$$G_1 = \frac{1}{lh}\left\{\frac{dF_s}{d\theta}\sqrt{g^{11}} + F_s\sqrt{g^{11}\left(g^{11}-1\right)}\right\} \quad [11]$$

$$G_2 = \left(\frac{F_s}{lh}\right)\sqrt{g^{11}} \quad [12]$$

where F_s is the shear force versus shear angle which can be approximated using a polynomial function of θ and $dF_s/d\theta$ is the gradient of the shear force versus shear angle curve which is also a function of θ.

4. Implementation of energy model

The energy model described in Section 2 requires the following material properties as input in order to generate shear force versus shear angle predictions: fibre volume fraction, matrix rheology, weave architecture and fibre diameter. For thermoplastic textile composites the matrix rheology is a function of shear strain rate and temperature. By specifying the temperature, the energy model allows prediction of a shear force surface in shear angle – angular velocity space. Using the input data for a 2 x 2 twill weave glass/polypropylene thermoplastic textile composite with a fibre volume fraction of 0.35 for which the matrix rheology has been characterised using an RMS 800 Rheometer, predictions have been made and found to give good comparison with experimental results (Harrison *et al*., 2004a). An example of the predicted shear force surface for this thermoplastic composite is shown in Figure 8. In order to incorporate these predictions in the FE code and consequently introduce rate dependency in the simulation, polynomial fits are made to the surface at specific angular velocities. In Figure 8, five different fits to the energy model predictions are indicated by the thick black lines superimposed on the shear force surface. The polynomial coefficients of these fits and corresponding angular velocities are stored in a matrix. This is the output of the energy model and is stored in a text file in a specified location on the computer. (Note that the text file containing the polynomial coefficients and corresponding angular velocities is the only output of the energy model, thus energy model parameters such as η_T and η_L are not required as input for the non-orthogonal model implemented in the FE code).

At the start of the FE simulation the output of the energy model is read in matrix format into a specified variable read by the subroutine. Care is taken to ensure that the code reads the data only one time, as repeated reading at each time step could slow the simulation significantly. (Increasing the number of polynomial curves fitted to the energy model predictions results in only a minor increase in the total simulation time). During the FE simulation the angular velocities of the individual finite elements are calculated in the user subroutine (a Fortran program containing the FE implementation of the non-orthogonal constitutive model). This is done for each element and at each time step of the simulation. The code uses the angular velocity of the element to determine which polynomial curve approximation of the shear force – shear angle (SF-SA) predictions will be used to calculate G_1 and G_2 using Equations [9] and [10]. This process is illustrated in Figure 8.

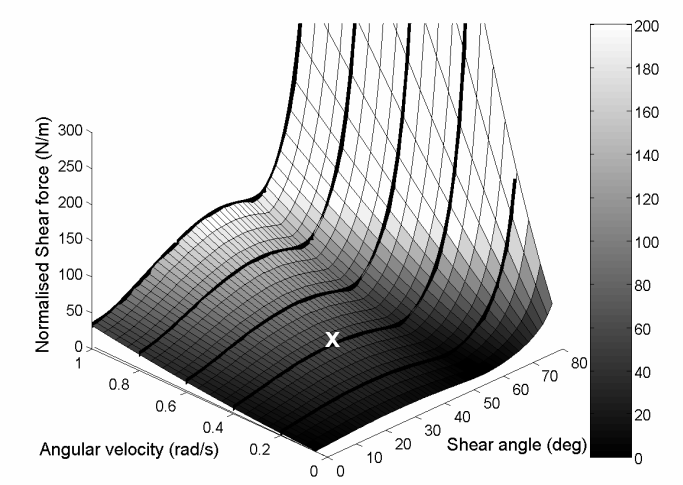

Figure 8. *Shear force – shear angle – angular velocity prediction for 2 x 2 twill weave glass/polypropylene thermoplastic textile composite at 190°C. Grey scale indicates the shear force magnitude of the surface (legend on right). The five thick black lines are 11th order polynomial fits to the surface at specific angular velocities: 0.2, 0.4, 0.6, 0.8 and 1 rads-1 (or 11, 22, 34, 46 $^o s^{-1}$). The white cross corresponds to the shear angle and angular velocity associated with a specific element (see text)*

The white cross on the shear force surface indicates the shear angle ($\approx 35^o$) and angular velocity (≈ 0.5 rads^{-1} or $29^o s^{-1}$) of a given element at a given time. In determining the shear parameters of this element, G_1 and G_2, the code assigns to the element the coefficients of the polynomial curve fitted at an angular velocity higher but contiguous with the angular velocity of the element. In this case the element would be assigned the polynomial coefficients of the 0.6 rads^{-1} (or $34^o s^{-1}$) curve.

5. Finite element results

FE results from simulations are presented which illustrate the combined implementation of the micro-mechanical and non-orthogonal constitutive models. The first simulation is of a Picture Frame test and uses the implicit FE method. This simulation provides a clear demonstration of the interfacing between the two models. Complex forming conditions associated with the press forming operation, such as contact between tool and blank, can be simulated more readily using the explicit FE method. Thus, explicit FE simulations are used to simulate the forming of both a hemisphere and a double dome geometry.

5.1. *Picture frame test simulations*

Implicit FE simulations of the Picture Frame test have been conducted using the interface described in Section 4. 100 quadrilateral linear membrane elements were used to model the blank. The boundary conditions imposed during the simulations were such that nodes along the sides of the material were constrained to move along the lines connecting the corner nodes. The bottom left corner was fixed while the upper right corner moved at a constant displacement rate in the diagonal direction.

Figure 9 shows the deformed mesh at different times during the simulation. The legend refers to the polynomial curve indicator value assigned by the interface to each element. Figure 10a shows the ideal shear angle expected in the case of inextensible fibres as the test proceeds, see Equation [13], together with the actual predicted shear angle from the FE simulation. Similarly, Figure 11b shows the ideal angular shear rate expected for the case of inextensible fibres, see Equation [14], together with the actual predicted angular shear rate produced by the FE simulation.

$$\theta = \frac{\pi}{2} - 2\arccos\left[\frac{1}{\sqrt{2}} + \frac{d}{2L}\right] \qquad [13]$$

$$\dot{\theta} = \frac{\dot{d}}{\sin\left(\pi/4 - \theta/2\right)} \qquad [14]$$

where d is the displacement of the upper right corner node, L is the side length of the blank (0.115 m) and the dot above the symbols indicates differentiation with respect to time.

Equation [14] shows that for a constant displacement rate the angular shear rate increases with increasing shear angle. Thus, during the course of the simulation the elements undergo progressively faster angular shear and are consequently assigned polynomial SF-SA curves of increasing value as the shear angle increases. In order to produce angular velocities corresponding to those typically induced during rapid press forming, a velocity scale factor has been introduced in the user subroutine. This

velocity scale factor affects the FE results only via its influence regarding assignment of polynomial SF-SA curves to the elements during the simulation. Otherwise the velocity scale factor has no bearing on the FE calculations. In this simulation 50 polynomial curves were fitted to energy model predictions at equal increments over an angular shear rate range of $\approx 10^o s^{-1}$ to $40^o s^{-1}$. Elements undergoing angular shear rates higher than $40^o s^{-1}$ were automatically assigned the highest polynomial SF-SA curve. The range of angular shear rates was chosen by referring to Figure 11b and imposed through the use of an appropriate velocity scale factor.

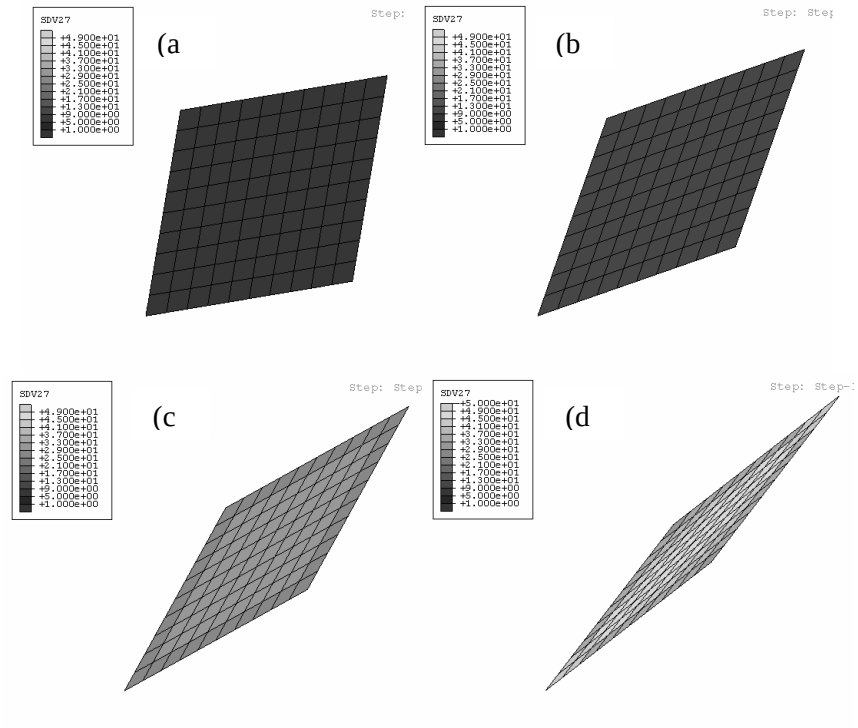

Figure 9. *Picture Frame test simulation at a shear angle of (a) 19^o (b) 38^o (c) 55^o and (d) 76^o. The grey scale indicates the value of the polynomial indicator value used by each element*

Figures 9 and 10 indicate the kinematic predictions of the simulation are correct until very high shear angles where mesh distortion is high. Figure 10a shows divergence from the ideal shear angle at about 70^o and Figure 10b shows a similar divergence in the angular shear rate at about 67^o. Thus the kinematics predictions of the non-orthogonal constitutive model are successful. Here, the emphasis is on examining the kinematic predictions of the code, force predictions of this model have been presented previously (Yu *et al*., 2005).

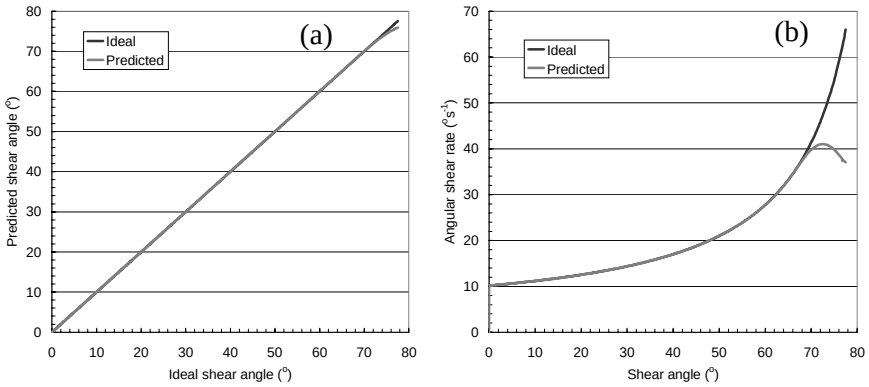

Figure 10. *Kinematics of ideal (black line) and simulated Picture Frame test (grey line). (a) Shear angle and (b) Angular shear rate. Simulation predictions were taken from a single element positioned near the centre of the blank*

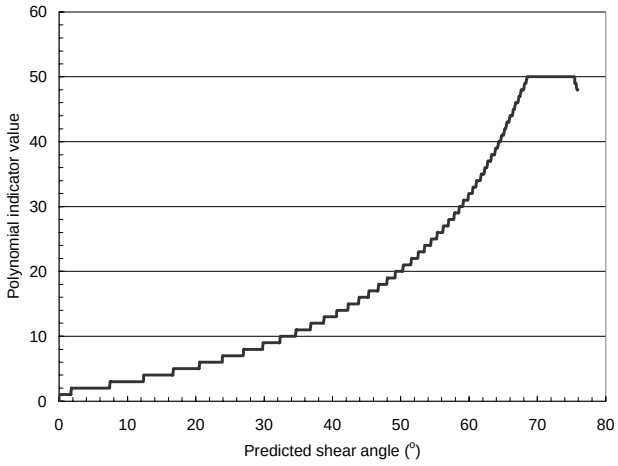

Figure 11. *Polynomial indicator value versus shear angle for centrally located element of Picture Frame simulation*

Figure 11 gives further insight into the operation of the interface. The value of the polynomial indicator curve assigned to one of the central elements of the blank is shown over the course of the simulation. Comparison of Figures 11 and 10b clearly shows the correlation between the change in the polynomial indicator value and the change in the angular shear rate of the element. This comparison demonstrates the correct functioning of the interface between the two models.

5.2. *Double dome forming simulations*

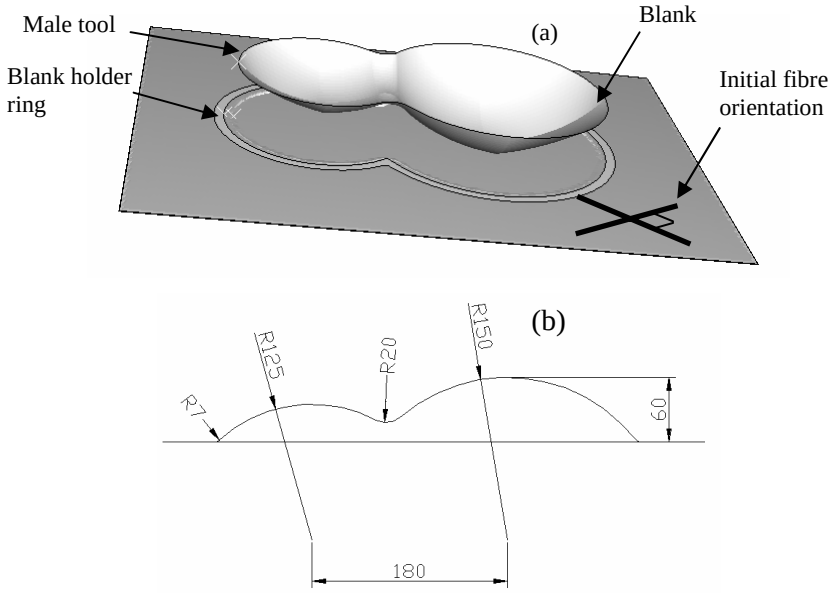

Figure 12. *(a) Double-dome forming simulation set-up showing male tool, blank holder ring and blank. A slightly larger matched female tool is positioned below the blank (3 mm gap between tools). Initial fibre orientation is shown on the blank. (b) Dimensions of the male tool in mm*

A simulation of a double-dome press forming process has been conducted. The set-up is shown in Figure 12a and the dimensions of the tool are shown in Figure 12b. The undeformed blank measured 650 x 450 mm and the initial fibre orientation is shown in Figure 12a. Figure 13 shows results from the simulation and consists of six images predicted from a single FE simulation. Rows correspond to different instances in time (0, 0.02, 0.04, 0.06 *s*, time increasing downwards) and columns correspond to: Left, magnitude of shear angle and Right, polynomial curve indicator value. 21,706 triangular linear reduced integration shell elements were used in creating the FE mesh of the blank. The indicator value is assigned to each element at the same time as the polynomial coefficients and, as with the Picture Frame simulation, serves to indicate which polynomial curve has been fitted to a given element. In this simulation the indicator value ranges from one to twenty. For convenience, a surface friction coefficient of 0.3 was chosen for all contact surfaces in the simulation and a blank holder force of 35N was applied. Areas of high shear are indicative of regions with relatively high angular shear rate. These areas can be seen to contain elements which have been assigned polynomial curves representing the shear behaviour of the textile composite at correspondingly high angular shear rates (see, Figure 13), as predicted by

the micro-mechanical energy model (Section 2). Figure 13 shows that in any given time step the polynomial indicator value changes considerably across the sheet in an apparently random and patchy manner. This is thought to be due to the nature of the explicit FE code solver. Each individual element may contain an error in any given time-step (12,000 in this simulation). However, the time averaged value of the angular velocity is shown to be correct through the reasonable prediction of the shear angle (left-hand column in Figure 13), *i.e*. the shear angle in each element is effectively the angular velocity of each element integrated over time.

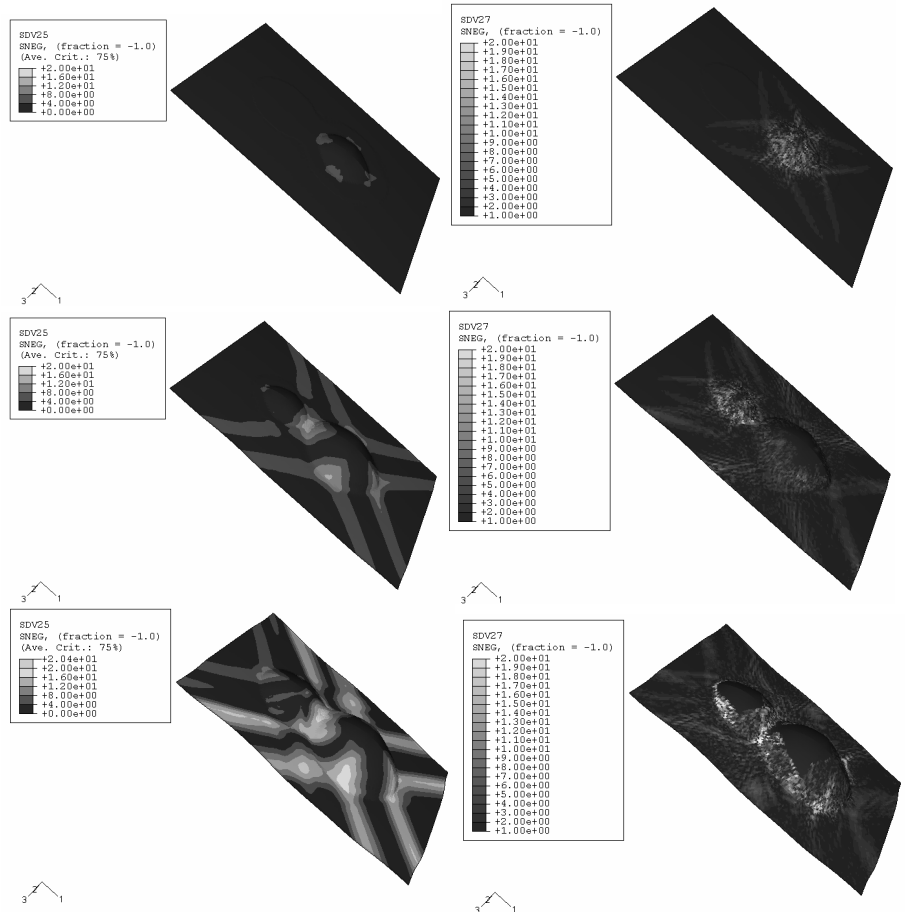

Figure 13. *FE simulation of double dome forming. Rows correspond to instances in time, (0, 0.02, 0.04, 0.06 s downwards) and columns correspond to: Left, magnitude of shear angle and Right, polynomial curve indicator value. The FE mesh of the blank is shown in the first time increment*

The double dome forming simulations demonstrate the basic philosophy behind this predictive approach to simulating the press form manufacture of viscous textile composites, *i.e*. predicting the shear behaviour of these materials using a micro-mechanical energy model and incorporating this behaviour in FE simulations of forming processes. Future work will involve examination of the force predictions of the Picture Frame test simulation and detailed investigation into the effects of rate and temperature dependent forming behaviour on the results of complex press forming operations. More realistic boundary conditions such as rate and temperature dependent tool-ply friction will also be incorporated in the simulations.

6. Conclusions

A constituent-based micro-mechanical energy model has been presented. SF-SA predictions of this model are based on the matrix rheology, fibre volume fraction and fabric architecture of the textile composite. As such the energy model is capable of predicting both the rate and temperature-dependent response of viscous textile composites due to shear. These SF-SA predictions have been incorporated in FE simulations via an interface implemented in the user subroutine. This interface is designed to pass energy model SF-SA predictions to a non-orthogonal constitutive model implemented in the FE code. This constitutive model uses the SF-SA energy model predictions to determine the shear stiffness of the finite elements. Rate dependency is produced in the FE simulations by automatically assigning appropriate SF-SA predictions to the finite elements according to the angular shear rate of the elements during the course of the simulation. Preliminary implicit FE simulations of the Picture Frame test have been presented which illustrate clearly the successful implementation of the interface in the FE code. Explicit FE simulations of forming simulations have also been conducted which indicate the current state of the work and suggest the future potential of the method.

Acknowledgements

We would like to thank the following organisations for their support: EPSRC, Ministry of Defence, University of Cambridge, DSTL Farnborough, ESI Software, Ford Motor Company Ltd., Granta Design Ltd, Hexcel Composites, MSC Software Ltd, Polynorm Plastics (UK) Ltd, Saint Gobain Vetrotex and the University of Twente and Cranfield University, for assistance in manufacture of the double dome tooling.

7. References

Boisse P., Gasser A., Hivet G., “Analyses of fabric tensile behaviour: determination of the biaxial tension-strain surfaces and their use in forming simulations”, *Composites: Part A*, 32, 2001, pp. 1395-1414.

Christensen R.M., "Effective viscous flow properties for fibre suspensions under concentrated conditions", *J Rheol*, 37/1, 1993, pp. 103-121.

Coffin D.W., Pipes R.B., Simacek P., "First-order approximations for the effective shearing viscosities of continuous-fiber suspensions", *J Compos Mater*, 29/9, 1995, pp.1196-1180.

Harrison P., Clifford M.J., Long A.C., Rudd C.D., "Constitutive modelling of impregnated continuous fibre reinforced composites: a micro-mechanical approach", *Plast Rubber Compos*, 2/31, 2002, pp. 76-86.

Harrison P., Clifford M.J., Long A.C., Rudd C.D., "A constitutive model for pre-impregnated viscous textile composites", *Composites: Part A*, 38, 7-8, 2004a, pp. 915-931.

Harrison P., Clifford M.J., Long A.C. "Shear characterisation of woven textile composites: a comparison between picture frame and bias extension experiments", *Comp. Sci. Tech.*, 64, 10-11, 2004b, pp. 1453-1465.

Hsiao S.W., Kikuchi N., "Numerical analysis and optimal design of composite thermoforming process", *Comput. Methods in Appl. Mech. Engrg.*, 177, pp. 1-34, 1999.

Lamers E.A.D., Akkerman R., Wijskamp S., "Drape Modelling of Multi-Layer Fabric Reinforced Thermoplastic Laminates", *Proc. 6th International Conference on Textile Composites (TexComp 6)*, Philadelphia, USA, September 2002b.

Lamers E.A.D., Wijskamp S., Akkerman R., "Drape Modelling of Multi-Layered Composites", *6th International ESAFORM Conference on Material Forming*, Salerno, April 28-30th, 2003, pp. 823-826.

Long A.C., Rudd C.D., "A simulation of reinforcement deformation during the production of preforms for liquid moulding processes", *J. Eng. Manuf., Proc. IMechE (Part B*), 208 1994, pp. 269-278.

Martin T.A., Bhattacharyya D., Collins I.F., "Bending of fibre-reinforced thermoplastic sheets", *Compos Manuf*, 6, 1995, pp. 177-187.

McGuiness G.B., O'Bradaigh C.M., "Characterisation of thermoplastic composite melts in rhombus-shear: the picture frame experiment", *Comp Part A-App S*, 29A, 1998, pp. 115-132.

Spencer A.J.M., "Theory of fabric-reinforced viscous fluids", *Comp Part A-App S A*, 31, 2000, pp. 1311-1321.

McGuiness G.B., O'Bradaigh C.M., "Development of rheological models for forming flows and picture frame testing of fabric reinforced thermoplastic sheets", *J Non-Newton Fluid*, 73, 1997, pp. 1-28.

McGuiness G.B., Canavan R.A., Nestor T.A., O'Bradaigh M.O., "A picture frame intra-ply sheet forming of composite materials", *Proc. ASME Materials Division, ASME*, 1995, pp. 1107-1118.

Pickett A.K., Queckborner T., De Luca P., Haug E., "An explicit finite element solution for the forming prediction of continuous fibre-reinforced thermoplastic sheets", *Composites Manufacturing*, 6, 1995, pp. 237-243.

Robertson R.E., Hsiue H.S., Sickafus E.N., Yeh G.S.Y., "Fibre rearrangements during the modelling of continuous fibre composites I: flat cloth to a hemisphere", *Polymer Composites*, 2, 1981, pp. 126-131.

Rogers T.G., "Rheological characterisation of anisotropic materials", *Composites*, 20/1, 1989, pp. 21-27.

Shuler S.F., Advani S.G., "Transverse squeeze flow of concentrated aligned fibers in viscous fluids", *J Non-Newton Fluid*, 65, 1996, pp. 47-74.

Van West B.P., Luby, S.C., "Fabric draping simulation in composites manufacturing part I and II", *J. Adv. Materials*, April 1997, pp. 29-41.

Yu W.R., Pourboghrat F., Chung K., Zampaloni M., Kang T.J., "Non-orthogonal constitutive equation for woven fabric reinforced thermoplastic composites", *Comp Part A-App S*, 33, 2002, pp. 1095-1105.

Yu W.R., Harrison P., Long A.C., "Finite Element Forming Simulation for Non-crimp Fabrics using a Non-Orthogonal Constitutive Equation", (accepted, *Comp Part A-App S*, 2005.